IJCRT.ORG ISSN : 2320-2882
INTERNATIONAL JOURNAL OF CREATIVE RESEARCH THOUGHTS (IJCRT)
An International Open Access, Peer-reviewed, Refereed Journal

Study Of Effect of Slip Condition On VISCO-elastic MHD Oscillatory forced Convection flow in a vertical channel with heat radiation

Sumeet Upadhyay[1] , Prof.(Dr.) Harishikesh Pandey[2]

[1]Research Scholar Department Of Mathematics Jai Prakash University Chapra

[2]Department Of Mathematics, Kamla College Gopalganj, Jai Prakash University Chapra

Introduction

The fluid flow between parallel plates by means of Couette motion is a classical fluid mechanics problem that has applications in magnetohydrodynamic (MHD) power generators and pumps, accelerators, aerodynamics heating, electrostatic precipitation, polymer technology, petroleum industry, purification of crude oil, and also in many material processing applications such as extrusion, metal forming, continuous casting, wire and glass fiber drawing, etc. This problem has received considerable attention in the case of horizontal parallel plates [1] than vertical parallel plates. An analysis of flow formation in Couette motion between vertical parallel plates was presented by Schlichting and Gersten [2]. This problem is of fundamental importance as it provides the exact solution and reveals how the velocity profiles varies with time, approaching a linear distribution asymptotically, and how the boundary layer spreads throughout the flow field.

Free convection in vertical channels has been studied widely in the last few decades under different physical effects [3] due to its importance in many engineering applications such as cooling of electronic equipments, design of passive solar systems for energy conversion, cooling of nuclear reactors, design of heat exchangers, chemical devices and process equipment, geothermal systems and others. However, very few papers deal with free convection in Couette motion between vertical parallel plates. Singh [4] studied the effect of free convection in Couette motion. He has considered the unsteady free convective flow of a viscous incompressible fluid between two vertical parallel plates at constant but different temperatures and one of which is impulsively started in its own plane and the other is kept stationary. This problem was further extended for magnetohydrodynamic case by Jha [5].

Fully developed laminar free convection Couette flow between two vertical parallel plates with transverse sinusoidal injection of the fluid at the stationary plate and its corresponding removal by constant suction through the plate in uniform motion has been analyzed by Jain and Gupta [6]. The physical effect of external shear in the form of Couette flow of a Bingham fluid in a vertical parallel plane channel with constant temperature differential across the walls was investigated analytically by Barletta and Magyari [7]. Steady fully developed combined forced and free convection Couette flow with viscous dissipation in a vertical channel has been investigated analytically by Barletta *et al.* [8].

Mathematical formulation

The unsteady magnetohydrodynamic flow of an electrically conducting viscous incompressible non – Newtonian Bingham fluid bounded by two parallel non – conducting porous plates with thermal radiation considering the Hall Effect is studied.

1. The fluid is assumed to be laminar, incompressible and obeying a Bingham model and flows between two infinite horizontal plates located at the $y' = \pm h$ planes and extend from $x' = 0$ to ∞ and from $z' = 0$ to ∞.
2. The upper plate moves with a uniform velocity *Uo* while the lower plate is stationary. The upper and lower plates are kept at two constant temperatures $T'2$ and $T'1$ respectively with $T_2' > T_1'$.
3. The fluid is acted upon by a constant pressure gradient dp'/dx' in the x'-direction, and a uniform suction from above and injection from below which are applied at $t' > 0$.
4. A uniform magnetic field *Bo* is applied in the positive y'- direction and is assumed undisturbed as the induced magnetic field is neglected by assuming a very small magnetic Reynolds number.
5. The Hall Effect is taken into consideration and consequently a z'- component for the velocity is expected to arise.
6. It is assumed that the external electric field is zero and the electric field due to the polarization of charges is negligible.
7. The homogeneous chemical reaction of first order with rate constant between the diffusing species and the fluid is neglected.
8. The concentration of the diffusing species in the binary mixture is assumed to be very small in comparison with the other chemical species, which are present and hence Soret and Dufour effects are negligible.
9. The uniform suction implies that the y'- component of the velocity is constant. Thus, the fluid velocity vector is given by

$$v(y',t') = u'(y',t')\bar{i} + v_o\bar{j} + w'(y',t')\bar{k}$$

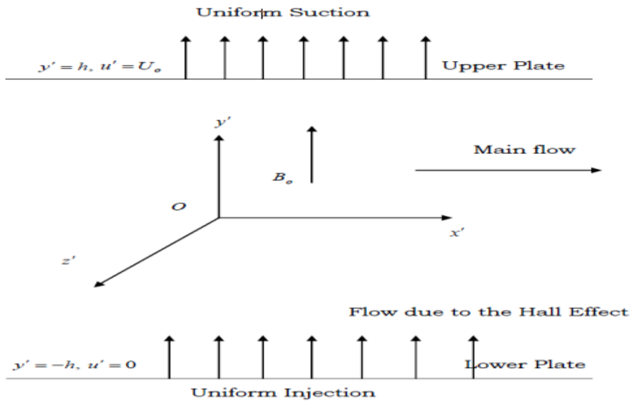

Figure 1: Geometry of the problem

It should be noted that the problem comes out to be a linear problem. In the hydrodynamic case without suction – injection, the problem reduces to Poiseuille problem [28] the classical hydrodynamic linear problem. Without suction – injection and by neglecting the Hall current, it reduces to Hartmann – Poiseuille problem [29], the classical MHD linear problem. The inclusion of the constant suction – injection as well as the Hall term [30] preserves linearity. So obviously does changing the Newtonian fluid to a non – Newtonian one in the present study. The classical problems (Poiseuille and Hartmann – Poiseuille) of channel flow and the related pipe flow of Newtonian fluid are known to be attainable in practice and to give results in excellent agreement with experiments. The fully developed profiles are observed away from the inlet and the side – walls of the channel. Using a non – Newtonian fluid is not expected to cause a problem.

Using a non – Newtonian fluid is not expected to cause a problem. The fluid motion starts from rest at *t*' = 0, and the no – slip condition at the plates implies that the fluid velocity has neither a *z*' nor an *x'*-component at *y' +-h*. The initial temperature of the fluid is assumed to be equal to *T'1*. Since the plates are infinite in the *x*' and *z*' -directions, the physical quantities do not change in these directions.

The flow of the fluid is governed by the momentum equation

$$\rho \frac{Dv}{Dt'} = \nabla.(\mu \nabla v) - \nabla p' + \bar{J} \times B_o \qquad (1)$$

Where ϱ the density of the fluid and μ is the apparent viscosity of the model and is given by

$$u' = K + \frac{\tau_o}{\sqrt{\left(\frac{\partial u'}{\partial y'}\right)^2 + \left(\frac{\partial w'}{\partial y'}\right)^2}} \qquad (2)$$

Where *K* the plastic viscosity of a Bingham fluid, *To* is the yield stress.

If the Hall term is retained, the current density *J* is given by

$$\bar{J} = \sigma\left[v \times B_o - \beta\left(\bar{J} \times B_o\right)\right] \tag{3}$$

Where σ is the electric conductivity of the fluid and β is the Hall factor. Equation (3) may be solved in *J* to yield

$$\bar{J} \times B_o = -\frac{\sigma B_o^2}{1+m^2}\left[\left(u' + mw'\right)\bar{i} + \left(w' - mu'\right)\bar{k}\right] \tag{4}$$

Where *m* is the Hall parameter and *m*= *σβBo* . Thus, the two components of the momentum equation (1) read

$$\rho\frac{\partial u'}{\partial t'} + \rho v_o \frac{\partial u'}{\partial y'} = -\frac{\partial p'}{\partial x'} + \frac{\partial}{\partial y'}\left(\mu\frac{\partial u'}{\partial y'}\right) - \frac{\sigma B_o^2}{1+m^2}\left(u' + mw'\right) \tag{5}$$

$$\rho\frac{\partial w'}{\partial t'} + \rho v_o \frac{\partial w'}{\partial y'} = \frac{\partial}{\partial y'}\left(\mu\frac{\partial w'}{\partial y'}\right) - \frac{\sigma B_o^2}{1+m^2}\left(w' - mu'\right) \tag{6}$$

Where $\frac{\partial p'}{\partial x'} = \frac{dp'}{dx'}e^{-at}$ is the unsteady pressure gradient

The energy equation with viscous and Joule dissipations is given by

$$\rho C_p \frac{\partial T'}{\partial t'} + \rho C_p v_o \frac{\partial T'}{\partial y'} = \kappa\frac{\partial}{\partial y'}\left(\frac{\partial T'}{\partial y'}\right) + \mu\left[\left(\frac{\partial u'}{\partial y'}\right)^2 + \left(\frac{\partial w'}{\partial y'}\right)^2\right] + \frac{\sigma B_o^2}{1+m^2}\left(u'^2 + w'^2\right) - \frac{\partial q_r}{\partial y'} \tag{7}$$

Where *Cp*, k and *D* are respectively, the specific heat capacity, the thermal conductivity and thermal diffusivity of the fluid. The second and third terms on the right – hand side of (7) represent the viscous and Joule dissipations respectively. We notice that each of these terms
has two components. This is because the Hall Effect brings about a velocity *w*' in the *z'*- direction.

The radiative heat flux term is simplified by making use of the Rosseland approximation [31] as

$$q_r = -\frac{4\bar{\sigma}}{3k^*}\frac{\partial T'^4}{\partial y'} \tag{8}$$

Here σ is Stefan – Boltzmann constant and *k** is the mean absorption coefficient. It is assumed that the temperature differences within the flow are sufficiently small so that *T'4* can be expressed as a linear function of *T*' after using Taylor"s series to expand *T'4* about the free stream temperature *T'1* and neglecting higher – order terms. This results in the following approximation:

$$T'^4 \cong 4T_1'^3 T' - 3T_1'^4 \tag{9}$$

Using equations (8) and (9) in the last term of equation (7), we obtain:

$$\frac{\partial q_r}{\partial y'} = -\frac{16\bar{\sigma}T_1'^3}{3k^*}\frac{\partial^2 T'}{\partial y'^2} \tag{10}$$

Introducing (10) in the equation (7), the energy equation becomes:

$$\rho C_p \frac{\partial T'}{\partial t'} + \rho C_p v_o \frac{\partial T'}{\partial y'} = \kappa \frac{\partial}{\partial y'}\left(\frac{\partial T'}{\partial y'}\right) + \mu\left[\left(\frac{\partial u'}{\partial y'}\right)^2 + \left(\frac{\partial w'}{\partial y'}\right)^2\right]$$
$$+ \frac{\sigma B_o^2}{1+m^2}\left(u'^2 + w'^2\right) + \frac{16\bar{\sigma} T_1^3}{3k^*}\frac{\partial^2 T'}{\partial y'^2}$$

(11)

The initial and boundary conditions of the problem are given by

$$\begin{Bmatrix} t' \le 0 : u' = w' = 0, T' = T_1' \ \ for\ all\ \ y' \\ t' > 0 : \begin{cases} u' = w' = 0, T' = T_1'\ at\ \ y' = -h \\ u' = U_o, w' = 0, T' = T_2'\ at\ \ y' = h \end{cases} \end{Bmatrix}$$

(11)

That the boundary conditions do not show dependence on *x'* suggests that the problem has a fully developed solution of the form:

$u' = u'(y', t'), v = v_o, p' = P + Gx'$

Where *P* is the pressure at *x*'= 0 (constant), *G* is the constant pressure gradient (negative). Under these conditions the continuity equation $\left(\frac{\partial u'}{\partial x'} + \frac{\partial v'}{\partial y'} = 0\right)$ is automatically satisfied. It is expedient to write the above equations in the non – dimensional form. To do this, we introduce the following non – dimensional quantities

$$x = \frac{x'}{h},\ y = \frac{y'}{h},\ z = \frac{z'}{h},\ t = \frac{t'U_o}{h},\ u = \frac{u'}{U_o},\ w = \frac{w'}{U_o},\ p = \frac{p'}{\rho U_o^2},\ \theta = \frac{T' - T_1'}{T_2' - T_1'},\ \bar{\mu} = \frac{\mu}{K},$$

$\tau_D = \frac{\tau_o h}{K U_o}$ is the Bingham Number (Dimensionless yield stress),

$\alpha = \frac{dp'}{dx'}$ is the pressure gradient,

$\mathrm{Re} = \frac{\rho U_o h}{K}$ is the Reynolds number,

$S = \frac{\rho v_o h}{K}$ is the suction parameter,

$\mathrm{Pr} = \frac{\rho C_p U_o h}{\kappa}$ is the Prandtl number,

$Ec = \frac{U_o K}{\rho C_p h (T_2' - T_1')}$ is the Eckert number,

$R=\dfrac{\kappa k^{*}}{4\sigma T_1'^{3}}$ is the thermal radiation parameter and

$M^2=\dfrac{\sigma B_o^2 h^2}{K}$ is the Hartmann number squared

In terms of the above non – dimensional variables and parameters equations (5) – (6) and (11) are, respectively, written as (where the hats are dropped for convenience)

$$\frac{\partial u}{\partial t}+\frac{S}{\mathrm{Re}}\frac{\partial u}{\partial y}=-\frac{dp}{dx}+\frac{1}{\mathrm{Re}}\left[\frac{\partial}{\partial y}\left(\mu\frac{\partial u}{\partial y}\right)-\frac{M^2}{1+m^2}(u+mw)\right] \tag{13}$$

$$\frac{\partial w}{\partial t}+\frac{S}{\mathrm{Re}}\frac{\partial w}{\partial y}=\frac{1}{\mathrm{Re}}\left[\frac{\partial}{\partial y}\left(\mu\frac{\partial w}{\partial y}\right)-\frac{M^2}{1+m^2}(w-mu)\right] \tag{14}$$

$$\frac{\partial \theta}{\partial t}+\frac{S}{\mathrm{Re}}\frac{\partial \theta}{\partial y}=\frac{1}{\mathrm{Pr}}\left(\frac{3R+4}{3R}\right)\frac{\partial}{\partial y}\left(\frac{\partial \theta}{\partial y}\right)+(Ec)\mu\left[\left(\frac{\partial u}{\partial y}\right)^2+\left(\frac{\partial w}{\partial y}\right)^2\right]+\frac{M^2(Ec)}{1+m^2}(u^2+w^2) \tag{15}$$

And the corresponding boundary conditions are

$$\begin{Bmatrix} t\le 0: u=w=\theta=0 \quad for\ all\ y \\ t>0:\begin{cases} u=w=\theta=0\ at\ \ y=-1 \\ u=1,\ w=0,\ \theta=1\ \ at\ \ y=1\end{cases}\end{Bmatrix} \tag{16}$$

Where $$\mu=1+\frac{\tau_D}{\sqrt{\left(\frac{\partial u}{\partial y}\right)^2+\left(\frac{\partial w}{\partial y}\right)^2}} \tag{17}$$

And $$\frac{dp}{dx}=\alpha e^{-at} \tag{18}$$

Numerical solution by Crank Nicholson Method

Equations (13), (14), (17) represent coupled system of non – linear partial differential equations which are solved numerically under the initial and boundary conditions (16) using the finite difference approximations. A linearization technique is first applied to replace the non – linear terms at a linear stage, with the corrections incorporated in subsequent iterative steps until convergence is reached. Then the Crank Nicholson implicit method is used at two successive time levels [32]. An iterative scheme is used to solve the linearized system of difference equations. The solution at a certain time step is chosen as an initial guess for next time step and the iterations are continued till convergence, within a prescribed accuracy. Finally, the resulting block tridiagonal system is solved using the generalized Thomas – algorithm.

The energy equation (15) is a linear non – homogeneous second order partial differential equation whose right-hand side is known from the solutions of the flow equations (13), (14), (17) subject to the conditions (16). The values of the velocity components are substituted in the right-hand side of equation (15) which is solved numerically with the initial and boundary conditions (16) using central differences and Thomas algorithm to obtain the temperature distribution. Finite difference equations relating the variables are obtained by writing the equations at the midpoint of the computational cell and then replacing the different terms by their second order central difference approximations in the y -direction. The diffusion terms are replaced by the average of the central differences at two successive time – levels. The computational domain is divided into meshes of dimension Δt and Δy in time and space respectively as shown in figure 5.2. We define the variables $B= uy$, $D= wy$ *and,* $L =\theta y$ to reduce the second order differential equations (13), (14), (17) to first order differential equations. The finite difference representations for the resulting first order differential equations (13), (14) take the following forms:

$$\left(\frac{u_{i+1,\,j+1}-u_{i,\,j+1}+u_{i+1,\,j}-u_{i,\,j}}{2(\Delta t)}\right)+\frac{S}{\mathrm{Re}}\left(\frac{B_{i+1,\,j+1}+B_{i,\,j+1}+B_{i+1,\,j}+B_{i,\,j}}{4}\right)=-\alpha e^{at}+\left(\frac{\overline{\mu}_{i+\frac{1}{2},\,j+\frac{1}{2}}}{\mathrm{Re}}\right)$$
$$\left(\frac{(B_{i+1,\,j+1}+B_{i,\,j+1})-(B_{i+1,\,j}+B_{i,\,j})}{2(\Delta y)}\right)+\left(\frac{\overline{\mu}'_{i+\frac{1}{2},\,j+\frac{1}{2}}}{\mathrm{Re}}\right)\left(\frac{B_{i+1,\,j+1}+B_{i,\,j+1}+B_{i+1,\,j}+B_{i,\,j}}{4}\right)-$$
$$\left(\frac{M^2}{1+m^2}\right)\left\{\left(\frac{u_{i+1,\,j+1}+u_{i,\,j+1}+u_{i+1,\,j}+u_{i,\,j}}{4\,\mathrm{Re}}\right)+m\left(\frac{w_{i+1,\,j+1}+w_{i,\,j+1}+w_{i+1,\,j}+w_{i,\,j}}{4\,\mathrm{Re}}\right)\right\} \tag{19}$$

$$\left(\frac{w_{i+1,\,j+1}-w_{i,\,j+1}+w_{i+1,\,j}-w_{i,\,j}}{2(\Delta t)}\right)+\frac{S}{\mathrm{Re}}\left(\frac{D_{i+1,\,j+1}+D_{i,\,j+1}+D_{i+1,\,j}+D_{i,\,j}}{4}\right)=\left(\frac{\overline{\mu}_{i+\frac{1}{2},\,j+\frac{1}{2}}}{\mathrm{Re}}\right)$$
$$\left(\frac{(D_{i+1,\,j+1}+D_{i,\,j+1})-(D_{i+1,\,j}+D_{i,\,j})}{2(\Delta y)}\right)+\left(\frac{\overline{\mu}'_{i+\frac{1}{2},\,j+\frac{1}{2}}}{\mathrm{Re}}\right)\left(\frac{D_{i+1,\,j+1}+D_{i,\,j+1}+D_{i+1,\,j}+D_{i,\,j}}{4}\right)-$$
$$\left(\frac{M^2}{1+m^2}\right)\left\{m\left(\frac{u_{i+1,\,j+1}+u_{i,\,j+1}+u_{i+1,\,j}+u_{i,\,j}}{4\,\mathrm{Re}}\right)-\left(\frac{w_{i+1,\,j+1}+w_{i,\,j+1}+w_{i+1,\,j}+w_{i,\,j}}{4\,\mathrm{Re}}\right)\right\} \tag{20}$$

Where $\overline{\mu}_{i+\frac{1}{2},\,j+\frac{1}{2}}=\dfrac{\overline{\mu}_{i+1,\,j+1}+\overline{\mu}_{i+1,\,j}+\mu_{i,\,j+1}+\mu_{i,\,j}}{4}$

and $\overline{\mu}'_{i+\frac{1}{2},\,j+\frac{1}{2}}=\dfrac{\overline{\mu}'_{i+1,\,j+1}+\overline{\mu}'_{i+1,\,j}+\mu'_{i,\,j+1}+\mu'_{i,\,j}}{4}$ (21)

The variables with bars are given initial guesses from the previous time step and an iterative scheme is used at every time to solve the linearized system of difference equations. Then the finite difference form for the energy equation (15) can be written as

$$\left(\frac{\theta_{i+1,\,j+1}-\theta_{i,\,j+1}+\theta_{i+1,\,j}-\theta_{i,\,j}}{2(\Delta t)}\right)+\frac{S}{\mathrm{Re}}\left(\frac{L_{i+1,\,j+1}+L_{i,\,j+1}+L_{i+1,\,j}+L_{i,\,j}}{4}\right)=$$
$$\frac{1}{\mathrm{Pr}}\left(\frac{3R+4}{3R}\right)\left(\frac{\left(L_{i+1,\,j+1}+L_{i,\,j+1}\right)-\left(L_{i+1,\,j}+L_{i,\,j}\right)}{4}\right)+QZFO \qquad (22)$$

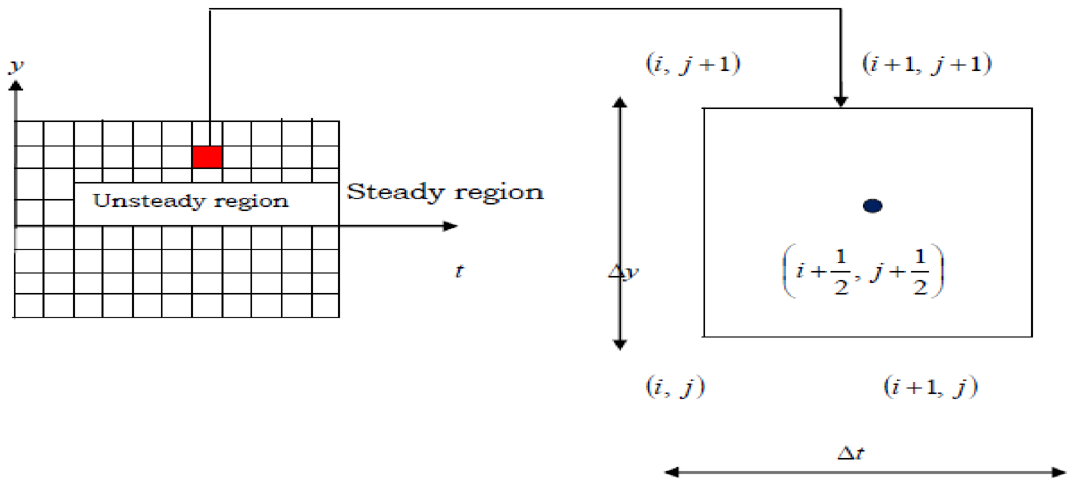

Figure 2: Mesh Layout

Where *QZFO* represents the Joule and viscous dissipation terms which are known from the solution of the momentum equations and can be evaluated at the midpoint $\left(i+\frac{1}{2},\ j+\frac{1}{2}\right)$ of the computational cell. Computations have been made for α =2.0, Pr = 0.71, Re = 2.0, M = 2.0, Ec = 0.03 and R = 2.0. Grid – independence studies show that the computational domain $0 < t < \infty$ and $-1<y<1$ can be divided into intervals with step sizes $\Delta t = 0.0001$ and $\Delta y = 0.005$ for time and space respectively. The truncation error of the central difference schemes of the governing equations is $O(\Delta t^2, \Delta y^2)$. Stability and rate of convergence are functions of the flow and heat parameters. Smaller step sizes do not show any significant change in the results. Convergence of the scheme is assumed when all of the unknowns u, B, w, D, θ and L for the last two approximations differ from unity by less than 10^{-6} for all values of y in $-1< y <1$ at every time step. Less than 7 approximations are required to satisfy this convergence criteria for all ranges of the parameters studied here.

Results and discussion

Figures 3 – 5 present the profiles of the velocity components *u* and *w* and the temperature θ respectively for various values of time *t* and for τ_D = 0, 0.05, and 0.1. The figures are evaluated for *M* =3.0, *m* = 3.0, *S* =1.0 and *R* = 2.0.

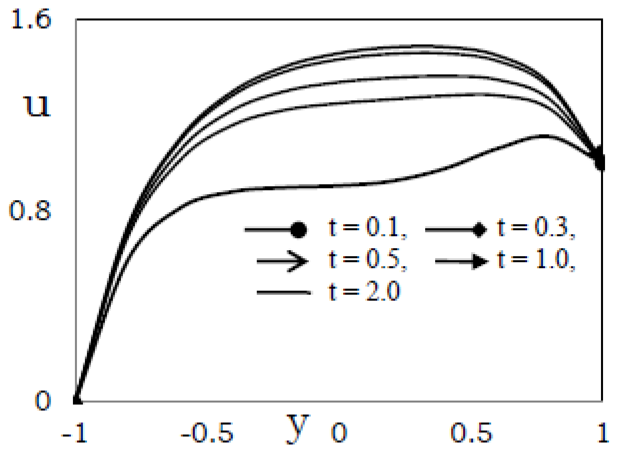

$(a)\ \tau_D = 0.0$

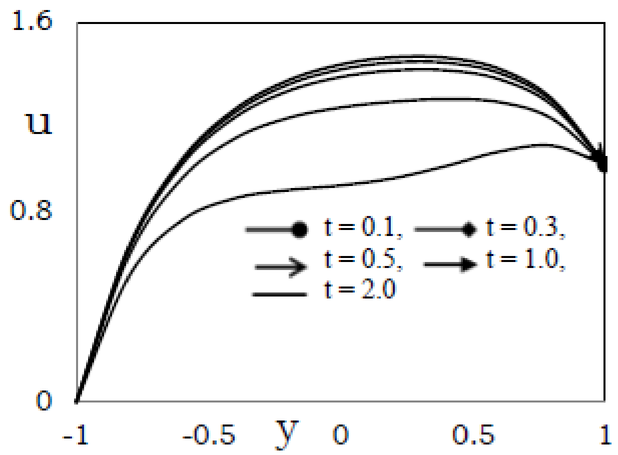

$(b)\ \tau_D = 0.05$

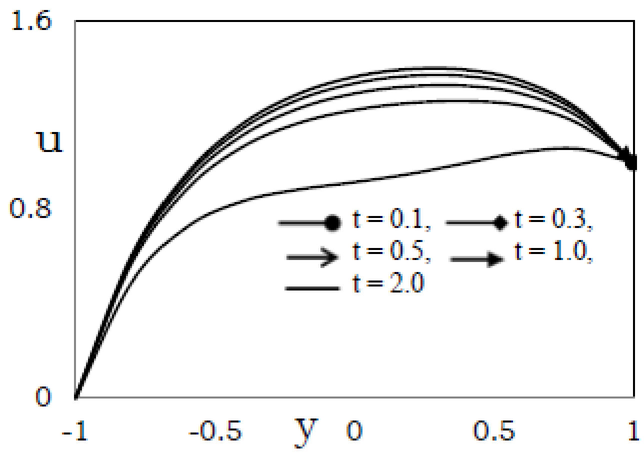

$(c)\ \tau_D = 0.10$

Figure 3: Time development of the velocity component *u* for *S* =1, *M* = 3

and *R* = 2

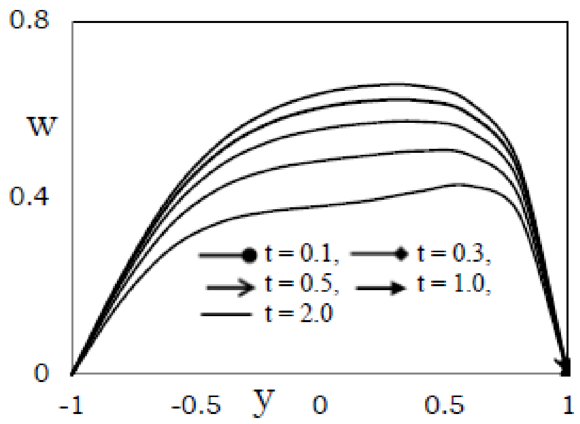

$(a)\ \tau_D = 0.0$

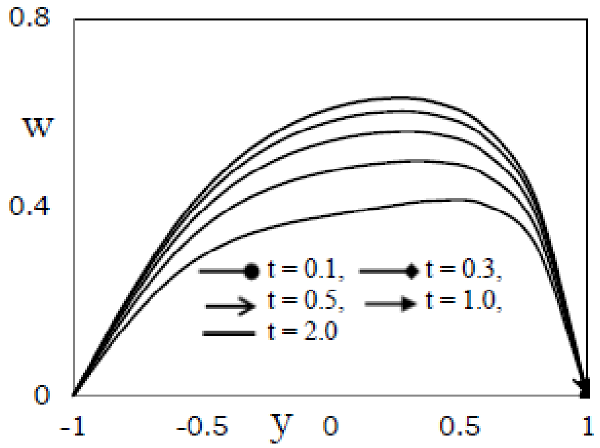

$(b)\ \tau_D = 0.05$

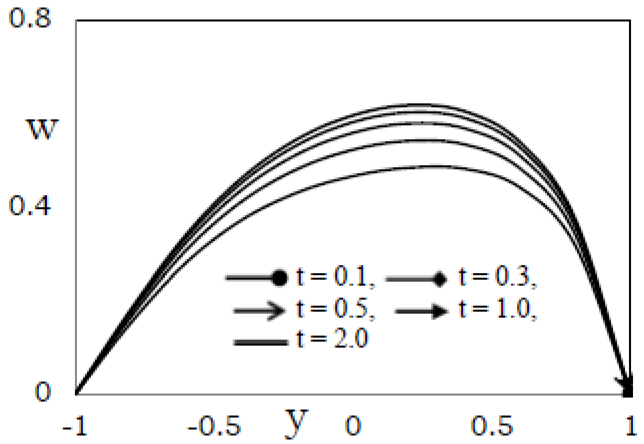

$(c)\ \tau_D = 0.10$

Figure 4: Time development of the velocity component w for *S=1, M=3, m=3 and R=2*

It is clear from figures 3 and figure 4 that increasing the yield stress τ_D decreases the velocity components u and w and the time at which they reach their steady state values as a result of increasing the viscosity. The figures show also that the velocity components u and w do not reach their steady state monotonically. Both u and w increase with time up till a maximum value and then decrease up to the steady state. This behaviour is more pronounced for small values of the parameter τ_D and it is clearer for *u* than for *w*.

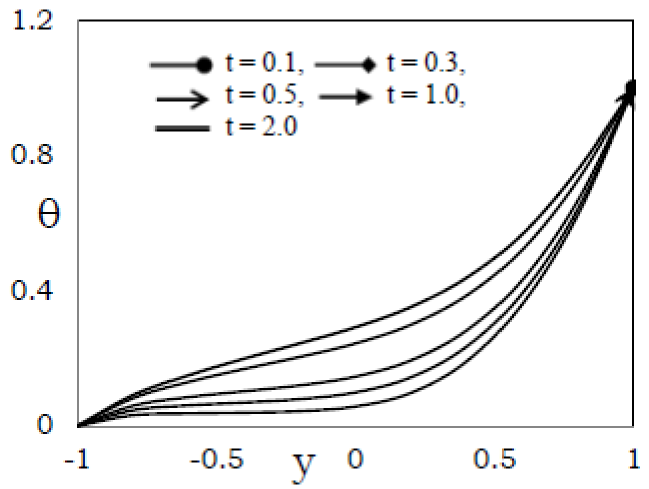

$(a)\ \tau_D = 0.0$

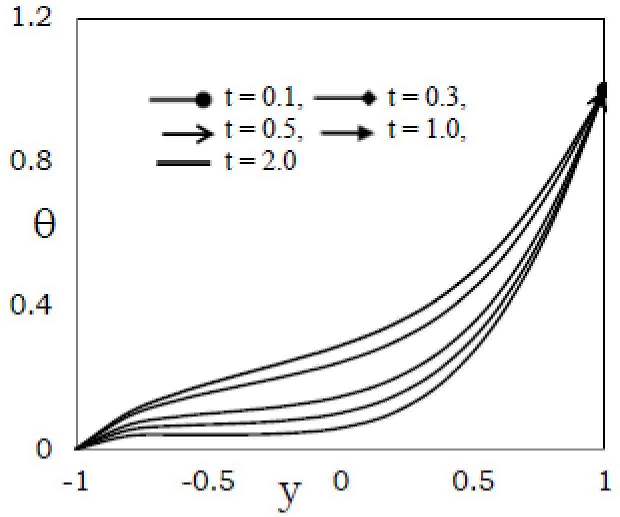

$(b)\ \tau_D = 0.05$

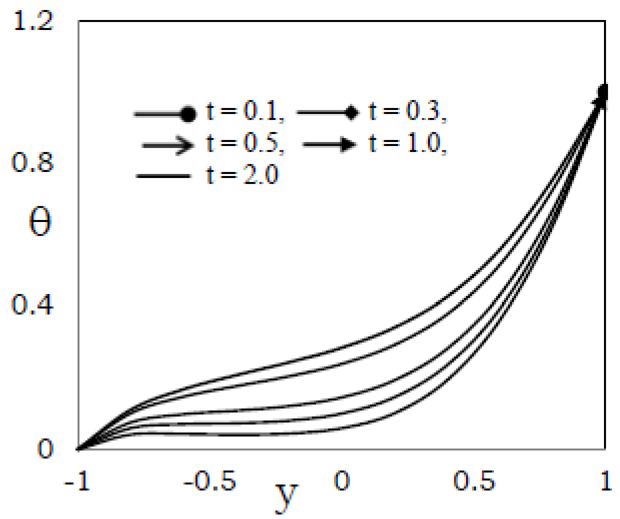

$(c)\ \tau_D = 0.10$

Figure 5.5: Time development of the temperature θ *for S=1, M=3, m=3 and R=2*

Figure 5 shows that the temperature profile reaches its steady state monotonically. It is observed also that the velocity component *u* reaches the steady state faster than *w* which, in turn, reaches the steady state faster than θ. This is expected as *u* is the source of *w*, while both *u* and *w* act as sources for the temperature.

Figures 6 – 8 depict the variation of the velocity components *u* and *w* and the temperature θ at the center of the channel (*y* = 0) with time respectively for various values of the Hall parameter *m* and for $\tau_{D}=$ 0, 0.05, and 0.1. In these figures *M* =3.0 and *S* =1.0.

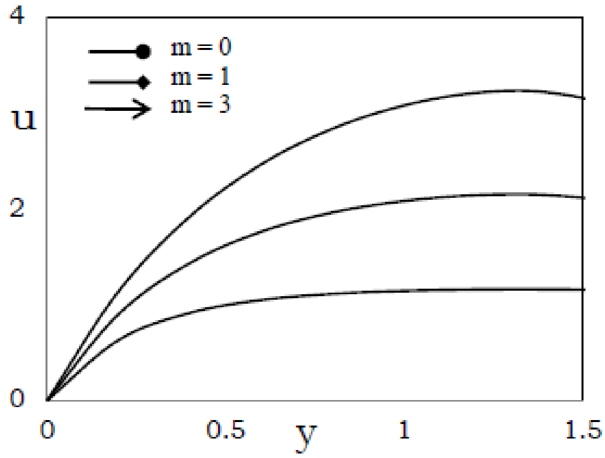

(*a*) $\tau_D = 0.0$

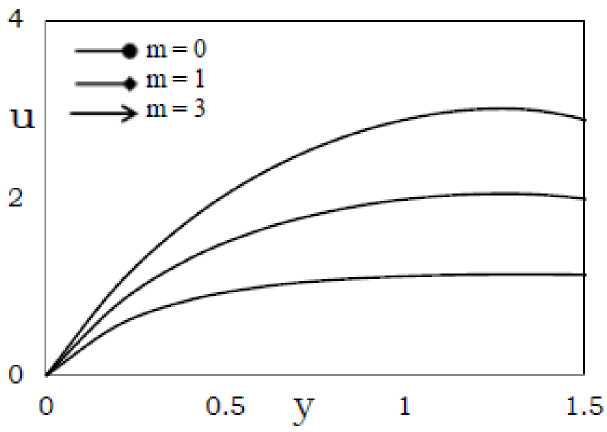

(*b*) $\tau_D = 0.05$

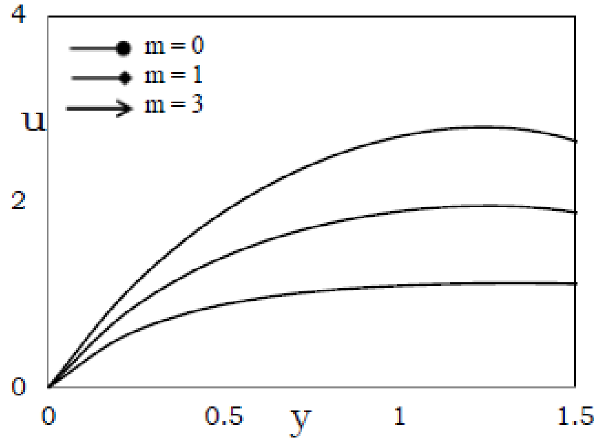

(c) $\tau_D = 0.10$

Figure 6: Effect of Hall parameter m on the time development of the velocity component μ *for S=1, M=3, m=3 and R=2*

Figure 6 shows that *u* increases with increasing *m* for all values of Ʈ$_D$ as the effective conductivity (=σ/(1+m2)) decreases with increasing *m* which reduces the magnetic damping force on *u*. It is observed also from the figure that the time at which *u* reaches its steady state value increases with increasing *m* while it decreases when Ʈ$_D$ increases. The effect of Ʈ$_D$ on *u* becomes more pronounced for large values of *m*.

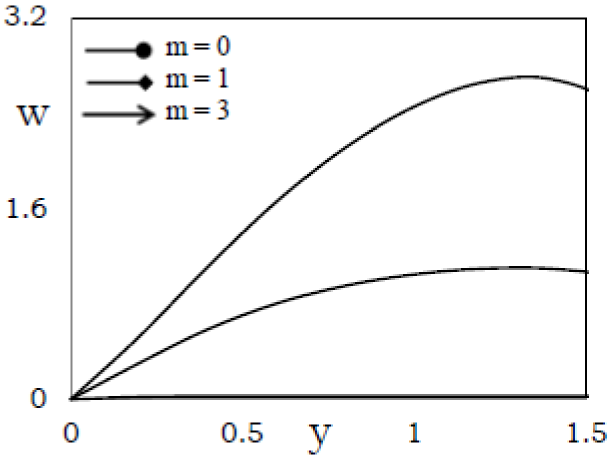

(a) $\tau_D = 0.0$

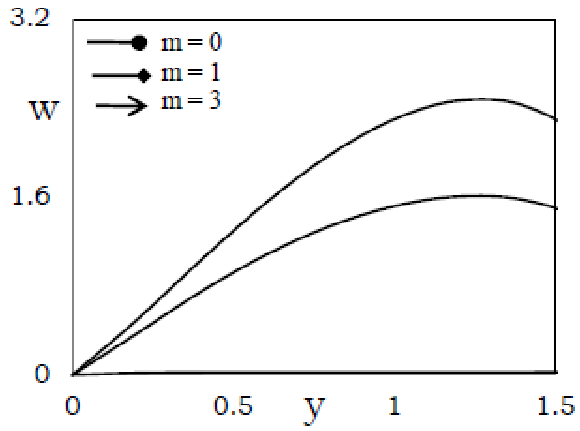

$(b)\ \tau_D = 0.05$

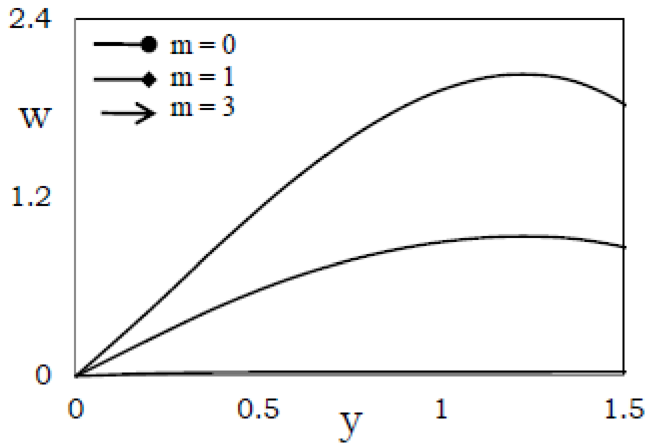

$(c)\ \tau_D = 0.10$

Figure 7: Effect of Hall parameter m on the time development of the velocity component w *for S=1, M=3, m=3 and R=2*

In figure 7 the velocity component *w* increases with increasing *m* as *w* is a result of the Hall Effect. On the other hand, at small times, *w* decreases when *m* increases. This happens due to the fact that, at small times *w* is very small and then the source term of *w* is proportional to $(mu/(1+m^2))$ which decreases with increasing *m (m* >1). This accounts for the crossing of the curves of *w* with *t* for all values of τ_D. Figures 6 and 7 indicate also that the influence of τ_D on *u* and *w* depends on *m* and becomes clearer when is *m* large. An interesting phenomenon is observed in Figures 6 and 7, which is that, when *m* has a non – zero value the component *u* and, sometimes, *w* overshoot. For some times they exceed their steady state values and then go down towards steady state. This may be explained by stating that with the progress of time, *u* increases and consequently *w* increases. According to equation (11) until *w* reaches its maximum value. The increase in *w* results in a small decrease in *u* according to equation (10). This reduction in *u* may, in turn, result in a decrease in *w* according to equation (11) which explains the reduction after the peaks. The time at which over shooting occurs decreases with increasing τ_D.

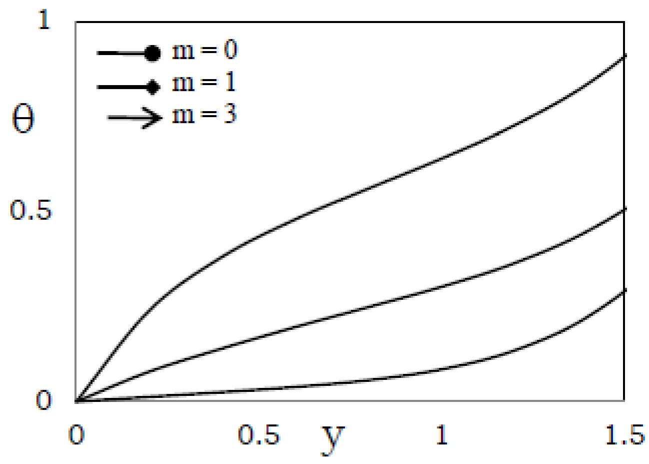

(a) $\tau_D = 0.0$

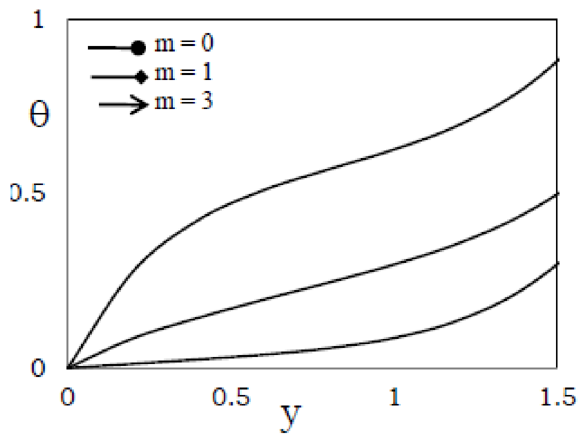

(b) $\tau_D = 0.05$

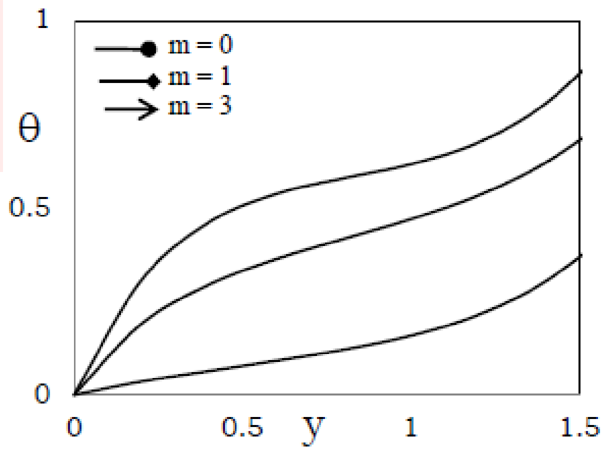

(c) $\tau_D = 0.10$

Figure 8: Effect of Hall parameter m on the time development of the temperature θ *for S=1, M=3, m=3 and R=2*

Figure 8 shows that the influence of m on θ depends on t. Increasing m decreases θ at small times and increases it at large times. This is due to the fact that, for small times, u and w are small and an increase in m increases u but decreases w. Then, the Joule dissipation which is also proportional to $(1/(1+m^2))$ decreases. For large times, increasing m increases both u and w and, in turn, increases the Joule and viscous dissipations. This accounts for the crossing of the curves of θ with time for all values of τ_D. It is also observed that increasing τ_D decreases the temperature θ for all values of *m*. This is because increasing τ_D decreases both *u* and *w* and their gradients which decreases the Joule and viscous dissipations. The figure shows also that the time at which θ reaches its steady state value increases with increasing *m* while it is not greatly affected by changing τ_D.

Figures 9 – 11 show the effect of the suction parameter *S* on the time development of the velocity components *u* and *w* and the temperature θ at *y* = 0 with time respectively for various values for τ_D =0.0, 0.05, and 0.1. In these figures *M* =3.0 and *m* = 3.0.

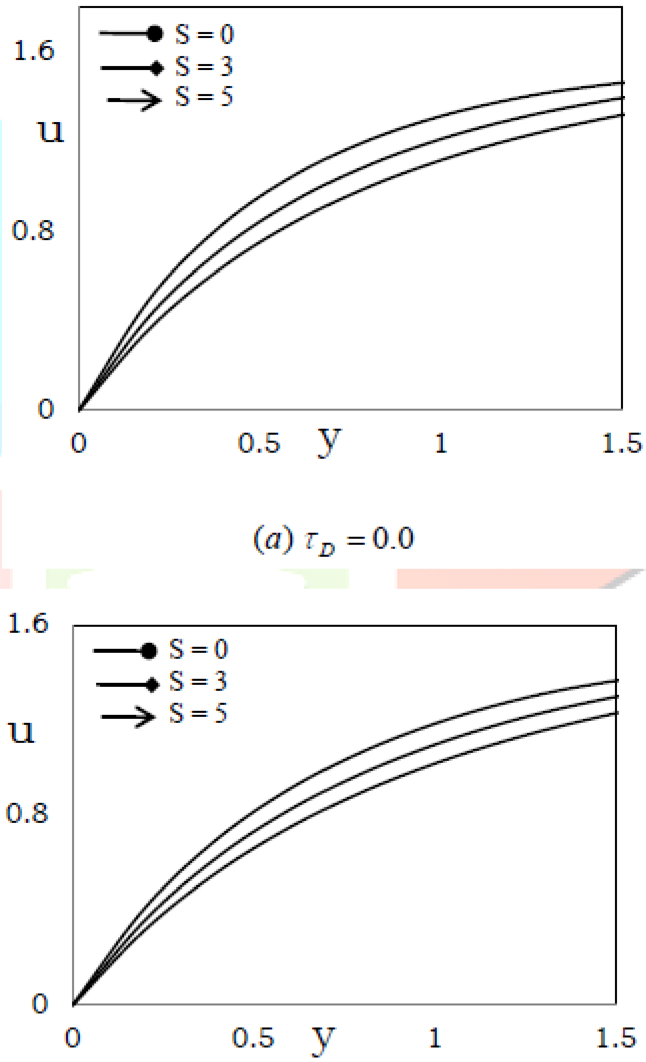

(a) $\tau_D = 0.0$

(b) $\tau_D = 0.05$

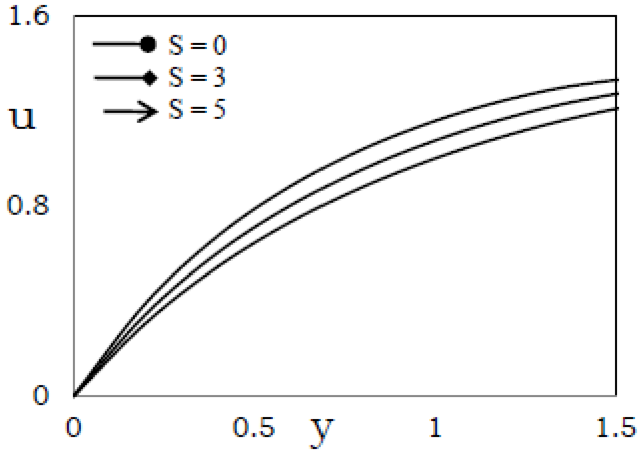

$(c)\ \tau_D = 0.10$

Figure 9: Effect of suction parameter S on the time development of the velocity component u *for M=3, m=3 and R=2*

Figure 9 shows that *u* at the center of the channel decreases with increasing *S* for all values of τ_D due to the convection of the fluid from regions in the lower half to the center, which has higher fluid speed.

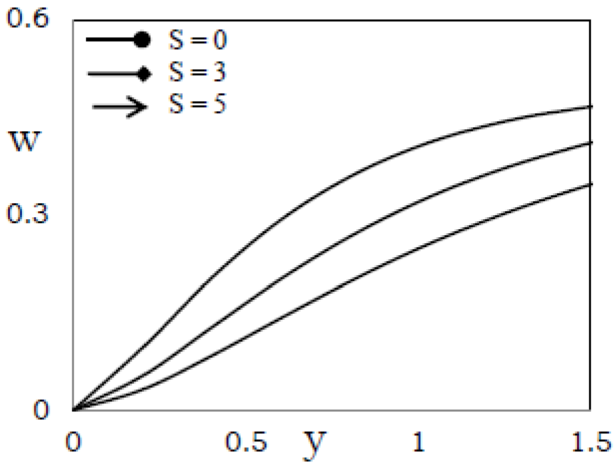

$(a)\ \tau_D = 0.0$

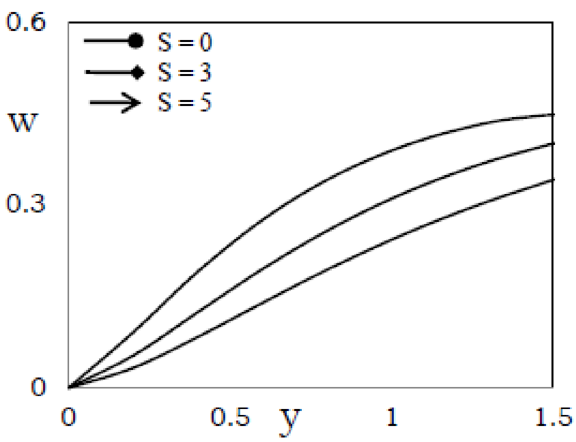

$(b)\ \tau_D = 0.05$

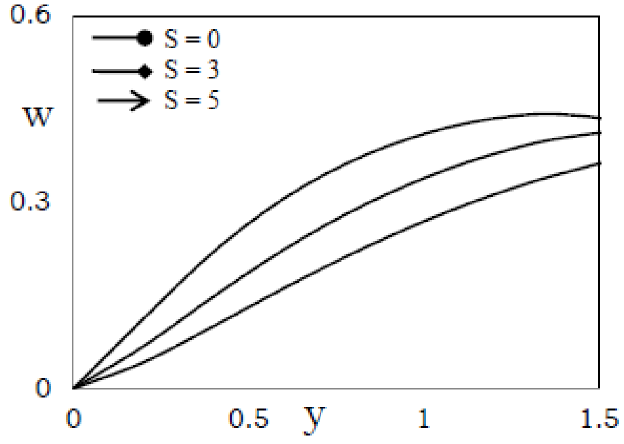

$(c)\ \tau_D = 0.10$

Figure 10: Effect of suction parameter S on the time development of the velocity component w *for M=3, m=3 and R=2*

Figure 10 overshooting in *w* especially for small values of τ_D.

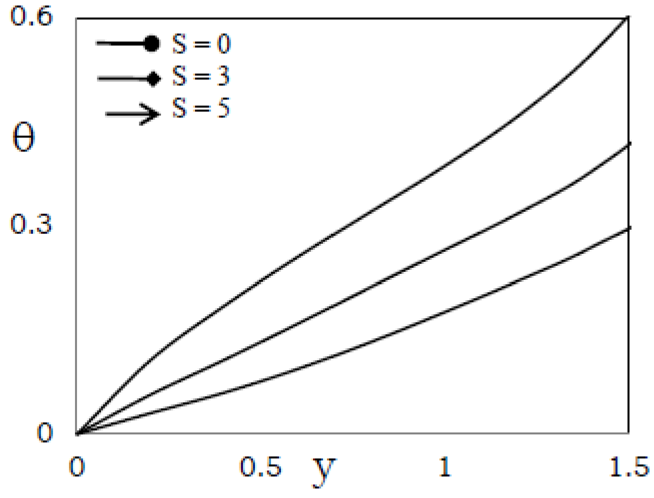

$(a)\ \tau_D = 0.0$

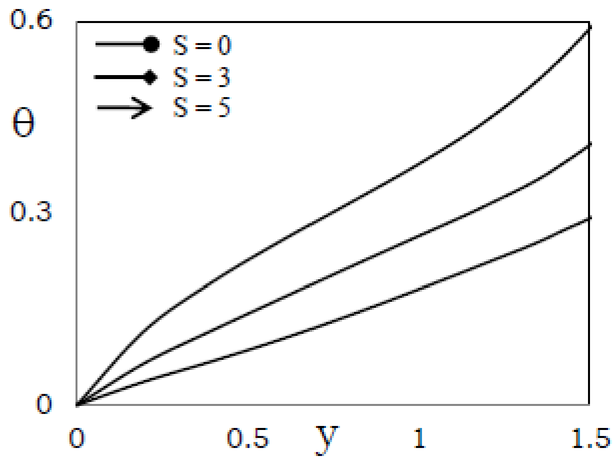

$(b)\ \tau_D = 0.05$

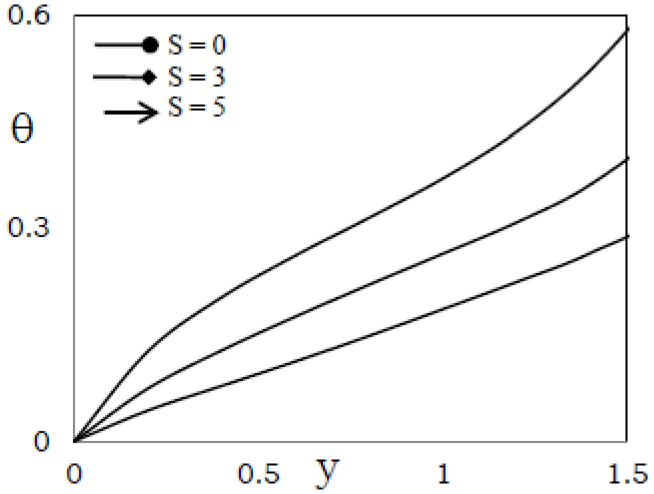

$(c)\ \tau_D = 0.10$

Figure 11: Effect of suction parameter S on the time development of the time development θ *for M=3, m=3 and R=2*

Figure 11 indicates that increasing *S* decreases the temperature at the center of the channel for all values of τ_D. This is due to the influence of the convection in pumping the fluid from the cold lower half towards the center of the channel.

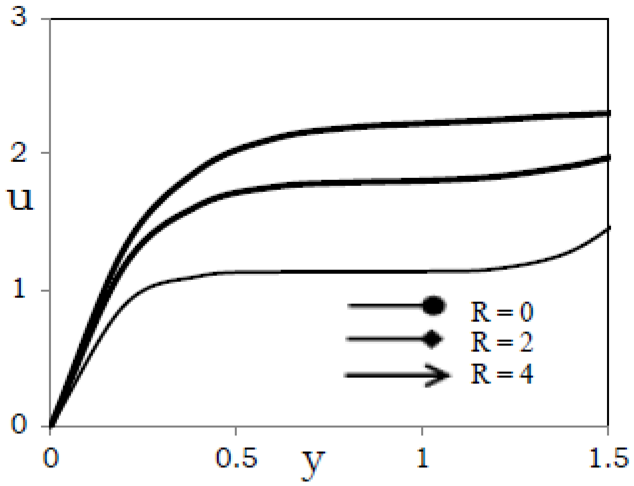

$(a)\ \tau_D = 0.0$

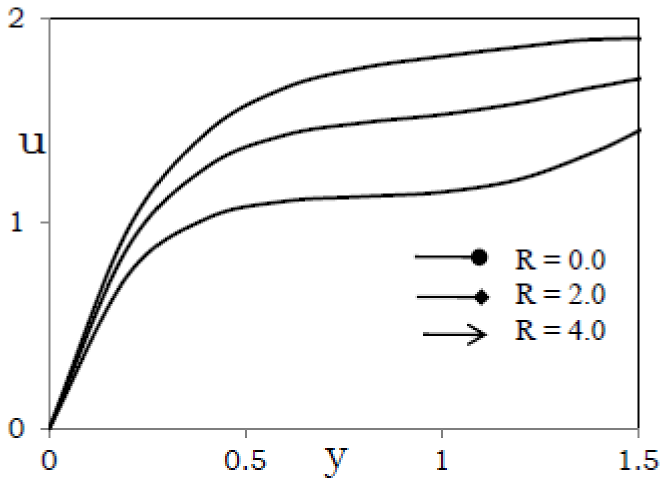

(b) $\tau_D = 0.05$

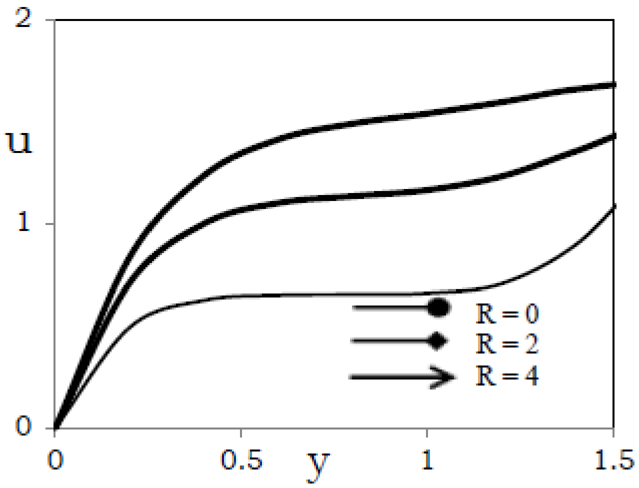

(c) $\tau_D = 0.10$

Figure 12: Effect of thermal radiation parameter R on the time development u *for M=3, m=3 and S=1*

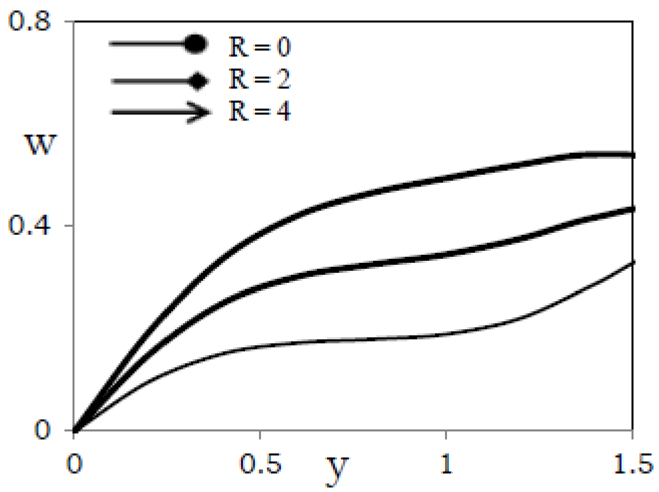

(a) $\tau_D = 0.0$

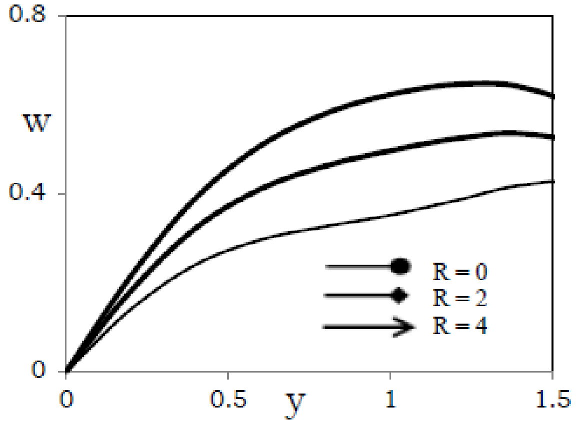

(b) $\tau_D = 0.05$

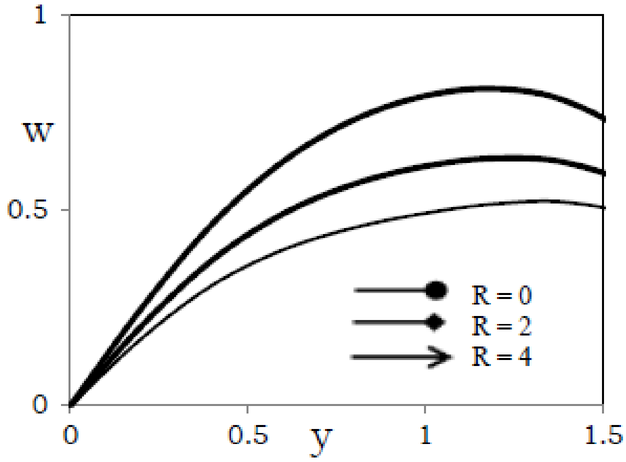

(c) $\tau_D = 0.10$

Figure 13: Effect of thermal radiation parameter R on the time development of velocity component w *for M=3, m=3 and S=1*

Figures (12) – (14) show the effect of the thermal radiation parameter R on the time development of the velocity components u and w and the temperature θ at y = 0 with time respectively for various values for $\tau_{D=}$ 0.0, 0.05, and 0.1. In these figures m = 3, M =3 and S =1. It is observed that increasing R decreases the velocity components and temperature of the fluid. An increase in the radiation emission, which is represented by R, reduces the rate of heat transfer through the fluid. This accounts for the decrease in temperature with increasing R. The velocity components are decreases through the reduction in buoyancy forces associated with the decreased temperature.

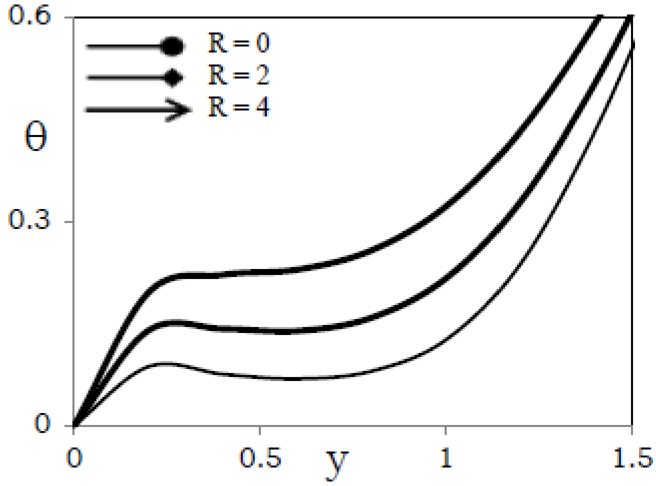

(a) $\tau_D = 0.0$

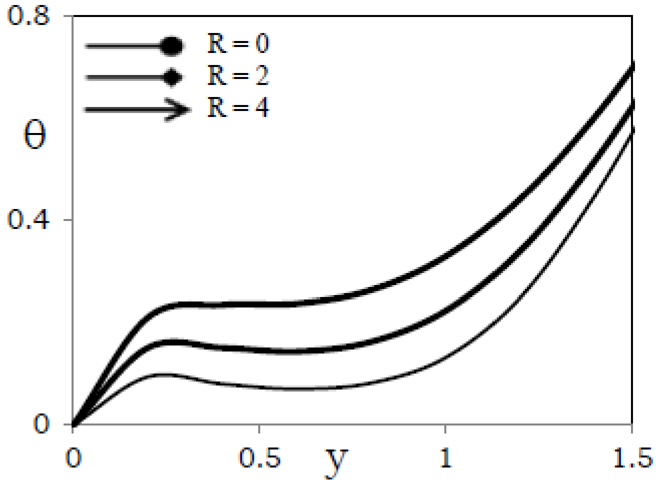

(b) $\tau_D = 0.05$

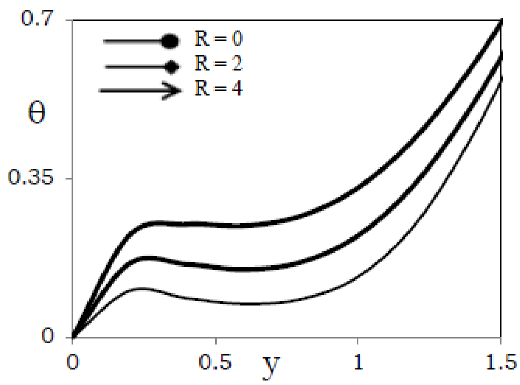

(c) $\tau_D = 0.10$

Figure 14: Effect of thermal radiation parameter R on the time development of temperature θ *for M=3, m=3 and S=1*

In order to examine the accuracy and correctness of the solutions, the results of the time development of the velocity components *u* and *w* at the center of the channel for the Newtonian case is compared and shown, as depicted Table 1, to have complete agreement with those reported by Attia. This ensures the satisfaction of all the governing equations; mass continuity, momentum and energy equations. While comparisons with previously published theoretical work on this problem were performed, no comparisons with experimental data were done because, as far as the author is aware, such data are lacking at the present time.

Table 1: Comparison of the present results and the known results of Attia [30] for Newtonian fluid ($\tau_{D=}$ 0.0) and R =0 for m = 3, M =3, S =1 and y = 0

t	Values of u		Values of w	
	Present results	Attia [201]	Present results	Attia [201]
0.1	0.4678	0.4669	0.0627	0.0619
0.2	0.8093	0.8089	0.2069	0.2056
0.3	1.0171	1.0160	0.3699	0.3687
0.4	1.1267	1.1251	0.5184	0.5171
0.5	1.1722	1.1708	0.6378	0.6370
0.6	1.1801	1.1791	0.7262	0.7260
0.7	1.1689	1.1682	0.7873	0.7872
0.8	1.1510	1.1495	0.8266	0.8263
0.9	1.1305	1.1297	0.8501	0.8491
1.0	1.1129	1.1122	0.8615	0.8607

Conclusions

A numerical solution to an unsteady magnetohydrodynamic the numerical solution of unsteady magnetohydrodynamic flow of an electrically conducting viscous incompressible non – Newtonian Bingham fluid bounded by two parallel non – conducting porous plates is studied with thermal radiation considering the Hall Effect have been derived. The dimensionless governing coupled, non – linear boundary layer partial differential equations are solved by an efficient, accurate, and extensively validated and unconditionally stable finite difference scheme of the Crank Nicholson method, which is more economical from a computational point of view. The effects of the Bingham number τ_D, the Hall parameter m, thermal radiation parameter R and the suction parameter S on the velocity and temperature distributions are studied. The Hall term affects the main velocity component u in the x - direction and gives rise to another velocity component w in the z -direction.

An overshooting in the velocity components u and w with time due to the Hall Effect is observed for all values of τ_D. The flow index τ_D has an apparent effect in controlling the overshooting in u or $w$and the time at which it occurs. The results show that the influence of the parameter τ_D on u and w depends on m and becomes more apparent when m is large. It is found also that the effect of m on w depends on t for all values of τ_D which accounts for a crossover in the w-t graph for various values of m. The effect of m on the magnitude of θ depends on n and becomes more pronounced in case of small τ_D.

The time at which *u* and *w* reach the steady state increases with increasing *m*, but decreases when τ_D increases. The time at which θ reaches its steady state increases with increasing *m* while it is not greatly affected by changing τ_D. The effect of thermal radiation parameter *R* on velocity components *u*, *w* and the temperature by changing the values of Bingham number τ_D. As thermal radiation parameter *R* increases, the velocity components *u*, *w* and temperature θ fields are decreases with increasing values of τ_D.

References

[1] Jana, R. N. and Datta, N., (1977). Couette flow and heat transfer in a rotating system, *Acta Mechanica*, Vol. 26, pp. 301 – 306. Schlichting, H. and Gersten, K., (2001). *Boundary – Layer Theory*, 8th Revised and Enlarged Edition, Springer.

[2] Narahari, M., (2009). Oscillatory plate temperature effects of free convection flow of dissipative fluid between long vertical parallel plates, *International Journal of Applied Mathematics and Mechanics*, Vol. 5, No. 3, pp. 30 – 46.

[3] Singh, A. K., (1988). Natural convection in unsteady Couette motion, *Defense Science Journal*, Vol. 38, No. 1, pp. 35 – 41.

[4] Jha, B. K., (2001). Natural convection in unsteady MHD Couette flow, *Heat and Mass Transfer*, Vol. 37, pp. 329 – 331.

[5] Jain, N. C. and Gupta, P., (2006). Three dimensional free convection Couette flow with transpiration cooling, *Journal of Zhejiang University Science A*, Vol. 7, No. 3, pp. 340 – 346.

[6] Barletta, A. and Magyari, E., (2008). Buoyant Couette – Bingham flow between vertical parallel plates, *International Journal of Thermal sciences*, Vol. 47, pp. 811 – 819.

[7] Barletta, A., Lazzari, S. and Magyari, E., (2008). Buoyant Poiseuille – Couette flow with viscous dissipation in a vertical channel, *ZAMP*, Vol. 59, pp. 1039 – 1056.

[8] Vradis, G. C., Dougher, J. and Kumar, S., (1993). Entrance pipe flow and heat transfer for a Bingham plastic, *Int. J. Heat Mass transfer*, Vol. 96, pp. 543 – 550.

[9] Petrov, A. G., (2000). The development of the flow of viscous and visco – plastic media between two parallel plates, *J. Appl. Math. Mech.*, Vol. 64, No. 1, pp. 123 – 132.

[10] Seddeek, M. A., (2002). Effects of radiation and variable viscosity on a MHD free convection flow past a semi – infinite flat plate with an aligned magnetic field in the case of unsteady flow, *Int. J. Heat and Mass Transfer*, Vol. 45, pp. 931 – 945.

[11] Viskanta, R. and Grosh, R. J., (1962). Boundary layer in thermal radiation absorbing and emitting media, *Int. J. Heat and Mass Transfer*, Vol. 5, pp. 795 – 806.

[12] Cess, R. D., (1966). The interaction of thermal radiation with free convection heat transfer, *Int. J. Heat and Mass Transfer*, Vol. 9, pp. 1269 – 1277.

[13] Sparrow, E. M. and Cess, R. D., (1966). *Radiation heat transfer*, Belmont, Calif.: Brooks/Cole.

[14] Howell, J. R., Siegel, R. and Menguc¸ M. P., (2010). *Thermal radiation heat transfer*, 5th ed. FL: CRC Press.

[15] Takhar, H. S., Gorla, R. S. R. and Soundalgekar, V. M., (1966). Short communication radiation effects on MHD free convection flow of a gas past a semi – infinite vertical plate, *Int. J. Numer. Methods Heat Fluid Flow*, Vol. 6, pp. 77 – 83.

[16] Raptis, A. and Massalas, C. V., (1998). Magnetohydrodynamic flow past a plate by the presence of radiation, *Heat Mass Transfer*, Vol. 34, pp. 107 – 109.

[17] Chamkha, A. J., (2000). Thermal radiation and buoyancy effects on hydromagnetic flow over an accelerating permeable surface with heat source or sink, *Int. J. Engg. Sci.*, Vol. 38, pp. 1699 – 1712.

[18] Cookey, C. I., Ogulu, A. and Omubo – Pepple, V. B., (2003). Influence of viscous dissipation and radiation on unsteady MHD free convection flow past an infinite heated vertical plate in a porous medium with time – dependent suction, *Int. J. Heat and Mass Transfer*, Vol. 46, pp. 2305 – 2311.

[19] Ogulu, A. and Makinde, O. D., (2008). Unsteady hydromagnetic free convection flow of a dissipative and radiating fluid past a vertical plate with constant heat flux, *Chem. Engg. Commun.*, Vol. 196, pp. 454 – 462.

[20] Mahmoud, M. A. A., (2009). Thermal radiation effect on unsteady MHD free convection flow past a vertical plate with temperature dependent viscosity, *Can. J. Chem. Engg.*, Vol. 87, pp. 47 – 52.

[21] Pop, I. and Watanabe, T., (1994). Hall Effect on magnetohydrodynamic free convection about a semi – infinite vertical flat plate, *Int. J. Engg. Sci.*, Vol. 32, pp. 1903 – 1911.

[22] Abo – Eldahab, E. M. and Elbarbary, E. M. E., (2001). Hall current effect on magnetohydrodynamic free convection flow past a semi – infinite vertical plate with mass transfer, *Int. J. Engg. Sci.*, Vol. 39, pp. 1641 – 1652.

[23] Takhar, H. S., Roy, S. and Nath, G., (2003). Unsteady free convection flow over an infinite vertical porous plate due to the combined effects of thermal and mass diffusion, magnetic field and Hall currents, *Heat Mass Transfer*, Vol. 39, pp. 825 – 834.

[24] Saha, L. K., Siddiqa, S. and Hossain, M. A., (2011). Effect of Hall current on MHD natural convection flow from vertical permeable flat plate with uniform surface heat flux, *Appl. Math. Mech. Engl. Ed.*, Vol. 32, No. 9, pp. 1127 – 1146.